Systematic Transitions of Tiling Patterns Formed by ABC Star-Shaped Terpolymers

Kenichi Hayashida,[†] Atsushi Takano,[†,‡] Shigeo Arai,[§] Yuya Shinohara,[||] Yoshiyuki Amemiya,[||] and Yushu Matsushita*,[†]

Department of Applied Chemistry, Graduate School of Engineering, Nagoya University, Nagoya 464-8603, Japan, Precursory Research for Embryonic Science and Technology (RESTO), Japan Science and Technology Agency, 4-1-8 Honcho, Kawaguchi 332-0012, Japan, EcoTopia Science Institute, Nagoya University, Nagoya 464-8603, Japan, and Department of Advanced Materials Science, Graduate School of Frontier Sciences, University of Tokyo, Chiba 277-8561, Japan

Received August 12, 2006; Revised Manuscript Received October 27, 2006

ABSTRACT: New tiling patterns with complex arrangements have been identified for ABC star-shaped terpolymers and ABC/A/B copolymer/homopolymer blends characterized by transmission electron microscopy and microbeam small-angle X-ray scattering. The samples are composed of polyisoprene (I), polystyrene (S), and poly(2-vinylpyridine) (P), whose volume ratios of I:S:P are 1.0:1.8:*X*, where *X* covers the range $0.8 \le X \le 3.2$. The other series of the type $I_{1.0}S_YP_{2.0}$ with *Y* in the range of $1.1 \le Y \le 2.7$ was also prepared by adding I or S homopolymers to the terpolymers of the type $I_{1.0}S_{1.8}P_X$. The systematic phase transition takes place in both series when the *X* or *Y* variables are increased and four new tiling patterns have been observed: [5.3, 5.3, 8], [4.5, 6, 9], [5, 5, 10], and [4, 6.7, 10], where the three numbers in the brackets denote the average coordination number (ACN) for the I, S, and P components, respectively. A very simple transition rule has been established: the ACN of the ascendant component increases monotonically with an increase of the variable *X* or *Y*, accompanied by the monotonic decrease in the ACN for the descendant component, which is polyisoprene in these cases.

Introduction

It is known that block and graft copolymers with incompatible components exhibit periodic nanophase-separated structures in condensed states due to the strong repulsion forces among the different chemical components.[1−4] The nanophase-separated structures adopt various morphologies such as spherical, cylindrical, bicontinuous, and lamellar structures in a volume fraction-dependent manner. Attention has been recently focused on experimental[5−15] and theoretical[16−23] investigations of ABC star-shaped terpolymers as a result of the attractive nanophase-separated structures that arise from the restricted connectivity among the component chains.

If the three components are immiscible with each other, the ABC star-shaped terpolymers typically adopt characteristic cylinder-based phase-separated structures because the geometrical restriction constrains the junction points to be aligned in a single dimension.[6,8−15] We previously reported that the characteristic cylindrical structures of ISP star-shaped terpolymers composed of polyisoprene (I), polystyrene (S), and poly(2-vinylpyridine) (P) were observed using transmission electron microscopy (TEM) and microbeam small-angle X-ray scattering (SAXS).[11,15] The cross-sections of the cylindrical structures reveal periodic tiling patterns consisting of even-numbered regular polygons, i.e., (6.6.6), (4.8.8), and (4.6.12), which are families of the 12 Archimedean tiling patterns.[24] For the ABC star-shaped terpolymers, only the three patterns mentioned above can exist in terms of the direct tiling manner because only three polygons can meet at a vertex and only even-numbered polygons should appear as proposed in the even-polygon theorem.[17] Recently, a more complex (3.3.4.3.4) tiling pattern was identified for an ISP star-shaped terpolymer system.[13,15] In this pattern, two types of nanodomains with different sizes and shapes are formed by one polymer component, which represents the first such observation for ABC star-shaped polymer systems. If such complexity is allowed for the ABC star-shaped terpolymers unexceptionally, additional tiling patterns with complex arrangements may exist for different compositions. ABC star-shaped polymer samples with various compositions are required for exploration of new tiling patterns. Unfortunately, the process of preparation of ABC star molecules with exact compositions represents difficult and time-consuming work.

On the other hand, methods of blending homopolymers with block copolymers have been used to produce various compositions, which allows for precise control of the composition. A block copolymer−homopolymer blend system has been studied extensively for polystyrene-*b*-isoprene (S-*b*-I) and styrene homopolymer (hS) blends.[25−29] The experimental results were categorized into three cases according to the locations of the hS chains. When the molecular weight of the hS is much smaller than that of the S block, $M_h \ll M_b$, (where M_h and M_b refer to the molecular weights of the hS and the S block, respectively), the hS dissolves uniformly into the corresponding block. If the molecular weight of the hS increases and reaches that of the block chain, i.e., $M_h \approx M_b$, the homopolymer tends to localize at the center of the nanodomains. When M_h exceeds M_b, the homopolymer begins to separate from the block copolymers and causes macrophase separation. Thus, we can control morphology of block copolymers by blending homopolymers unless the molecular weights of the homopolymers are greater than the molecular weights of the corresponding blocks.[25,26,30,31] With regard to simulations, new phases have been predicted by blending of homopolymers, which have never been subsequently identified in neat block copolymers.[32−35] In these studies, the

* To whom all correspondence should be addressed. E-mail: yushu@apchem.nagoya-u.ac.jp. Telephone: +81-52-789-4605. Fax: +81-52-789-3210.
[†] Department of Applied Chemistry.
[‡] Precursory Research for Embryonic Science and Technology (RESTO).
[§] EcoTopia Science Institute.
[||] Department of Advanced Materials Science.

10.1021/ma0618474 CCC: $33.50
Published on Web 12/05/2006

Scheme 1

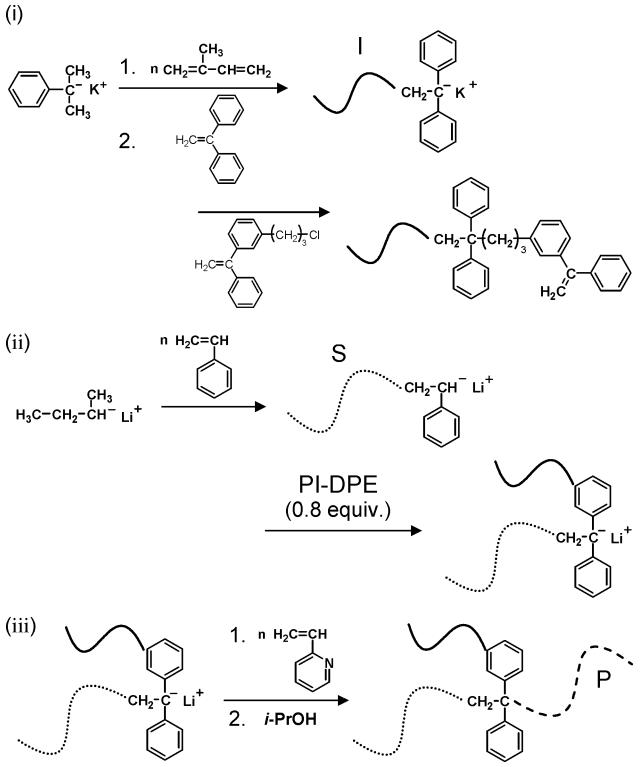

molecular weights of the added homopolymers were comparable to the molecular weights of the corresponding blocks, which stabilized the specific morphologies as a result of the localizations of the homopolymers.

In this work, homopolymers with molecular weights much smaller than those of the corresponding blocks were used to tune the compositions of ISP star block copolymers in order to prevent stabilization of certain morphologies arising from specific localization of the homopolymers. First, the five ISP star-shaped terpolymers whose volume ratios of I:S:P is 1.0:1.8:*X*, where *X* covers the range $0.8 \leq X \leq 3.2$, were synthesized and additional six blend samples were prepared by mixing two ISP star polymers. Another series of the type $I_{1.0}S_YP_{2.0}$ with *Y* being in the range $1.1 \leq Y \leq 2.7$ was also prepared by blending I or S homopolymers with $I_{1.0}S_{1.8}P_X$. The structures of the solvent-cast films were investigated by transmission electron microscopy (TEM) and microbeam small-angle X-ray scattering (SAXS). We identified new tiling patterns with complex arrangements in addition to regular Archimedean tiling patterns. Transitions of all tiling patterns observed in this work were categorized according to a simple rule.

Experimental Section

Materials. *sec*-Butyllithium was purchased from Asia Lithium Co. Ltd. and diluted with purified *n*-hexane., The three monomers, i.e., isoprene, styrene, and 2-vinylpyridine, and 1,1-diphenylethylene (DPE) were purified by previously established methods using tetrahydrofuran (THF) as the solvent.[36,37] Isopropanol was distilled over calcium hydride. Cumylpotassium[38] and 1-[*o*-(3-chloropropyldimethylsilyl)phenyl]-1-phenylethylene (DPE-Cl)[39] were synthesized by previously reported methods. The DPE dimeric dianion potassium salt (DPE_2K_2) was prepared by a reaction of a solution of DPE in THF with a potassium mirror.

Synthesis of the ISP Star-Shaped Terpolymers. ISP star-shaped terpolymers were synthesized via three steps, as shown in Scheme 1. All operations were carried out in sealed glass apparatuses with break-seals, which had been degassed under pressures at or below 10^{-4} mmHg. Isoprene was first polymerized with cumylpotassium in THF at −78 °C. Introduction of a vinyl group on one chain end was effected by successive addition of a threefold excess of DPE and a fivefold excess of DPE-Cl. The polyisoprene with the DPE-type vinyl end group (PI-DPE) was separated by repeated precipitation into methanol. After drying, PI-DPE was sealed in a glass apparatus and dissolved in THF. A dilute solution of DPE_2K_2 in THF was added to the PI-DPE solution until the reddish color of the carbanion from DPE_2K_2 slightly remained. Successively, polystyryllithium (1.2 equiv), polymerized with *sec*-butyllithium in THF at −78 °C, was added to the PI-DPE solution and stirred for 2 days. Subsequently, the excess polystyryl anion was deactivated by allowing the preparation to stand at room temperature for 3 days.[9] Portions of the polyisoprene and the polystyrene preparations were isolated as precursors for later characterization. The polyisoprene−polystyrene coupled macroinitiator solution was divided into several portions. Finally, a controlled amount of a 2-vinylpyridine monomer in THF was added into the macroinitiator solution and polymerized at −78 °C. After termination with isopropanol, the solvent was removed by evaporation and the product was freeze-dried from a 1,4-dioxane solution. The dried crude star polymer preparation was rinsed with a mixed solvent of toluene/cyclohexane, 5:95 by volume, to effect a rough separation of the isoprene−styrene diblock copolymer and their homopolymers. The star polymer was further purified by SEC fractionations.[11] Using this procedure, five samples were prepared that have exactly the same I and S chains but with different poly(2-vinyl pyridine) (P) chains.

Table 1. Characteristics of the ISP Star-Shaped Terpolymers

sample	M_n (10^3)	M_w/M_n [a]	$\Phi_I:\Phi_S:\Phi_P$ [d]
polyisoprene	113.3[a]	1.04	
polystyrene	127.4[b]	1.01	
$I_{1.0}S_{1.8}P_{0.8}$	154.7[c]	1.02	1:1.79:0.83
$I_{1.0}S_{1.8}P_{1.4}$	163.3[c]	1.02	1:1.82:1.40
$I_{1.0}S_{1.8}P_{2.0}$	173.1[c]	1.02	1:1.79:1.96
$I_{1.0}S_{1.8}P_{2.5}$	180.3[c]	1.02	1:1.83:2.45
$I_{1.0}S_{1.8}P_{3.2}$	192.1[c]	1.02	1:1.83:3.17

[a] Determined by ^{1}H NMR. [b] Determined by SEC using polystyrene standard samples. [c] Estimated by ^{1}H NMR based on M_n of polystyrene. [d] Volume ratios of I:S:P calculated using bulk densities of the components, i.e., 0.926, 1.05, and 1.14 g/cm^3 for the I, S, and P components, respectively.

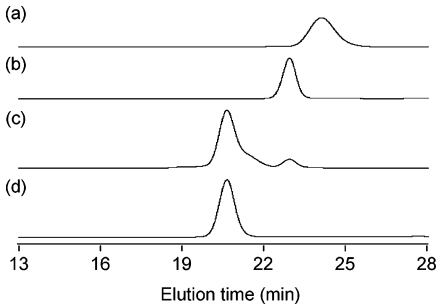

Figure 1. SEC curves of the polymerized products: (a) polyisoprene, (b) polystyrene, (c) crude reactant for $I_{1.0}S_{1.8}P_{2.0}$, (d) purified star-shaped terpolymer ($I_{1.0}S_{1.8}P_{2.0}$).

Characterization of the ISP Star-Shaped Samples. Table 1 summarizes the volume ratios of the three components in the ISP star-shaped terpolymers synthesized in this study together with their molecular weights and molecular weight distributions (MWDs). The compositions were determined using a 500 MHz ^{1}H NMR spectrometer (Varian Inc., Unity Inova 500). The volume ratios of I:S:P are 1:1.8:X, where *X* is in the range $0.8 \leq X \leq 3.2$. The number-average molecular weight of the common polystyrene and the MWDs of the polymer samples were determined by SEC using standard polystyrene samples. The analyses were carried out using a SEC system (Tosoh Ltd.) equipped with a set of three separation columns ($G4000_{HR}$ 300 mm × 7.8 mm i.d.) and a refractive index detector (RI-8021). Figure 1 compares the SEC curves of the polyisoprene (Figure 1a) and the polystyrene (Figure 1b) precursors and the $I_{1.0}S_{1.8}P_{2.0}$ star polymer (Figure 1d) together with that of

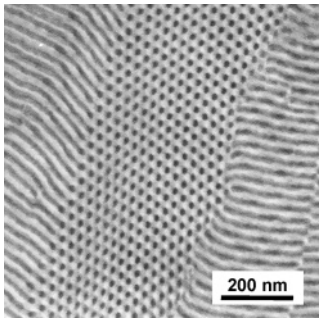

Figure 2. TEM image of a representative cylindrical structure formed by the $I_{1.0}S_{1.8}P_{1.0}$ star-shaped terpolymer.

Table 2. Blend Ratios of the ISP Star-Shaped Terpolymers and hI and hS to Obtain the $I_{1.0}S_{1.8}P_X$ and $I_{1.0}S_YP_{2.0}$ Series

series	sample	blending procedure	weight fraction	$\Phi_I:\Phi_S:\Phi_P$[a]
$I_{1.0}S_{1.8}P_X$	$I_{1.0}S_{1.8}P_{1.0}$	$I_{1.0}S_{1.8}P_{0.8}/I_{1.0}S_{1.8}P_{1.4}$	0.665/0.335	1:1.80:1.00
	$I_{1.0}S_{1.8}P_{1.2}$	$I_{1.0}S_{1.8}P_{0.8}/I_{1.0}S_{1.8}P_{1.4}$	0.340/0.660	1:1.81:1.18
	$I_{1.0}S_{1.8}P_{1.6}$	$I_{1.0}S_{1.8}P_{1.4}/I_{1.0}S_{1.8}P_{2.0}$	0.570/0.430	1:1.81:1.62
	$I_{1.0}S_{1.8}P_{1.8}$	$I_{1.0}S_{1.8}P_{1.4}/I_{1.0}S_{1.8}P_{2.0}$	0.277/0.723	1:1.80:1.75
	$I_{1.0}S_{1.8}P_{2.1}$	$I_{1.0}S_{1.8}P_{2.0}/I_{1.0}S_{1.8}P_{2.5}$	0.585/0.415	1:1.80:2.14
	$I_{1.0}S_{1.8}P_{2.9}$	$I_{1.0}S_{1.8}P_{2.5}/I_{1.0}S_{1.8}P_{3.2}$	0.344/0.656	1:1.83:2.91
$I_{1.0}S_YP_{2.0}$	$I_{1.0}S_{1.1}P_{2.0}$	$I_{1.0}S_{1.8}P_{3.2}$/hI	0.920/0.080	1:1.14:1.97
	$I_{1.0}S_{1.3}P_{2.0}$	$I_{1.0}S_{1.8}P_{2.5}/I_{1.0}S_{1.8}P_{3.2}$/hI	0.446/0.492/0.062	1:1.28:1.98
	$I_{1.0}S_{1.5}P_{2.0}$	$I_{1.0}S_{1.8}P_{2.5}$/hI	0.959/0.041	1:1.45:1.95
	$I_{1.0}S_{1.6}P_{2.0}$	$I_{1.0}S_{1.8}P_{2.0}/I_{1.0}S_{1.8}P_{2.5}$/hI	0.458/0.519/0.023	1:1.59:1.95
	$I_{1.0}S_{2.0}P_{2.0}$	$I_{1.0}S_{1.8}P_{2.0}$/hS	0.960/0.040	1:1.98:1.96
	$I_{1.0}S_{2.2}P_{2.0}$	$I_{1.0}S_{1.8}P_{2.0}$/hS	0.921/0.079	1:2.21:1.96
	$I_{1.0}S_{2.3}P_{2.0}$	$I_{1.0}S_{1.8}P_{2.0}$/hS	0.900/0.100	1:2.32:1.96
	$I_{1.0}S_{2.4}P_{2.0}$	$I_{1.0}S_{1.8}P_{2.0}$/hS	0.881/0.119	1:2.44:1.96
	$I_{1.0}S_{2.7}P_{2.0}$	$I_{1.0}S_{1.8}P_{2.0}$/hS	0.841/0.159	1:2.69:1.96

[a] Volume ratios of I:S:P calculated using bulk densities of the components, i.e., 0.926, 1.05, and 1.14 g/cm^3 for the I, S, and P components, respectively.

the crude product (Figure 1c) as an example. Two distinct contaminants are recognized on the SEC curve of the crude $I_{1.0}S_{1.8}P_{2.0}$ sample. The shoulder of the peak for the star-shaped terpolymer observed at approximately 21.5 min represents the deactivated IS diblock copolymer. The other peak at approximately 23.0 min represents the polystyrene precursor.

In contrast, a sharp and symmetric peak that indicates a narrow MWD is observed on the SEC curve for the purified $I_{1.0}S_{1.8}P_{2.0}$ sample, as shown in Figure 1d.

Preparation of the Blend Samples. Several other samples with volume ratios of $I_{1.0}S_{1.8}P_X$ and $I_{1.0}S_YP_{2.0}$ were prepared by blending star polymers or by blending homopolymers with star polymers, as shown in Table 2. The $I_{1.0}S_{1.8}P_X$ samples with X of 1.0, 1.2, 1.6, 1.8, 2.1, and 2.9 were prepared by blending the two parent samples with the most similar compositions. For example, $I_{1.0}S_{1.8}P_{1.0}$ was prepared by blending $I_{1.0}S_{1.8}P_{0.8}$ and $I_{1.0}S_{1.8}P_{1.4}$. To produce the $I_{1.0}S_YP_{2.0}$ samples, low-molecular-weight polyisoprene (hI) (M_n = 3 k) and polystyrene (hS) (M_n = 3 k) were separately added to the $I_{1.0}S_{1.8}P_X$ samples. For the range $Y < 1.8$, hI was added to the $I_{1.0}S_{1.8}P_X$ samples with $X > 2.0$ to obtain blend samples with Y of 1.1, 1.3, 1.5, and 1.6. For the range $Y > 1.8$, hS was added to $I_{1.0}S_{1.8}P_{2.0}$ to obtain the ISP star-based blend samples with Y of 2.0, 2.2, 2.3, 2.4, and 2.7.

Morphological Observations. Sample films were obtained by solvent casting from 5% solutions of the samples in THF for 2 days. The films were dried at room temperature for 12 h and annealed at 170 °C under a vacuum for 3 days. For TEM observations, the annealed samples were cut into ultrathin sections having a thickness range of 35−50 nm using an ultramicrotome (Reica, Ultracut FCS) with a diamond knife (Diatome, cryo T) at room temperature. The sections were successively stained with osmium tetroxide and iodine. Osmium tetroxide stains I heavily, while iodine stains P intermediately. The stained films were observed on a transmission electron microscope (Hitachi, H-800) operated at an accelerating voltage of 100 kV.

For microbeam SAXS measurements,[15] the annealed sample films were cut into thin sections having an approximate thickness of 30 μm using the same ultramicrotome system. The microbeam SAXS measurements were performed using beamline BL40XU at the SPring-8 facility (Hyogo, Japan). The wavelength of the X-ray was 0.12 nm, and the size of the X-ray microbeam was approximately 5 μm × 5 μm (fwhm). The precise camera length was calibrated to 2.75 m with a standard collagen sample.

Results

Two-Dimensional Tiling Patterns of $I_{1.0}S_{1.8}P_X$. Figure 2 shows a TEM image for an ultrathin section of $I_{1.0}S_{1.8}P_{1.0}$ star-shaped terpolymer as a typical example. Because the sample was stained with osmium tetroxide and iodine for the TEM observation, the black, white, and gray domains represent the I, S, and P components, respectively. Cylindrical morphology is easily recognized in the cross-sectional and side views of the cylindrical array. Figure 3 shows the cross-sectional TEM images of the cylindrical structures for the $I_{1.0}S_{1.8}P_X$ (X = 1.0, 1.6, 2.0, and 2.9) and the corresponding schematic tiling patterns. As shown in Figure 3a, $I_{1.0}S_{1.8}P_{1.0}$ has a honeycomb-type structure, which has also been observed in previous investigations of the $I_{1.0}S_{1.0}P_{0.7}$ star-shaped terpolymer.[11] In this tiling pattern, each hexagonal domain contacts the other 6 domains, the component I, S, and P form the 6-coordinated domains, and the three hexagons meet at all vertices in a (6.6.6) Archimedean tiling pattern. In the same manner, the tiling pattern of $I_{1.0}S_{1.8}P_{2.9}$, where the components I, S, and P have the 4-, 6-, and

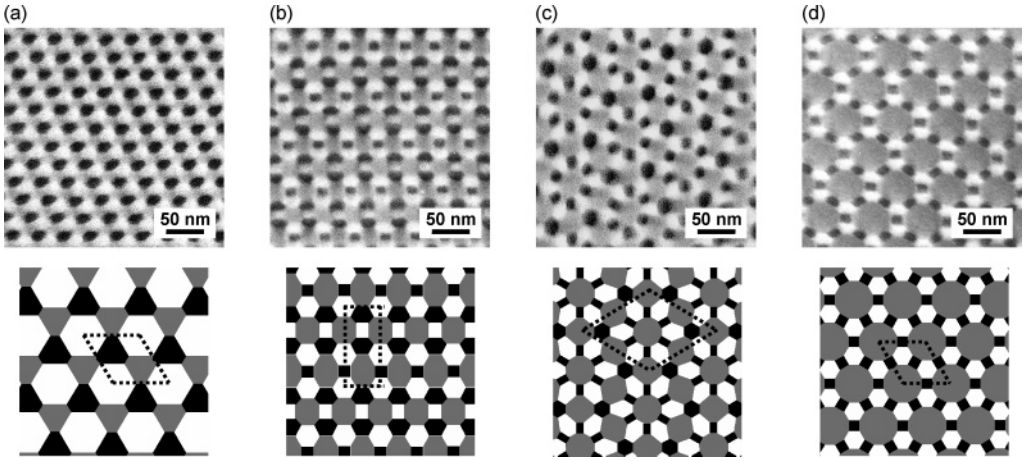

Figure 3. TEM images of the four ISP star-shaped terpolymer samples (top) and the corresponding schematic tiling patterns (bottom): (a) $I_{1.0}S_{1.8}P_{1.0}$, (b) $I_{1.0}S_{1.8}P_{1.6}$, (c) $I_{1.0}S_{1.8}P_{2.0}$, (d) $I_{1.0}S_{1.8}P_{2.9}$.

Table 3. Characteristics of the Tiling Patterns for the Star Polymers of the $I_{1.0}S_{1.8}P_X$ Series[a]

$I_1S_{1.8}P_X$	$X = 0.8, 1.0, 1.2, 1.4$	$X = 1.6, 1.8$	$X = 2.0$	$X = 2.1, 2.5, 2.9$
I	6-coord. × 1 (6)	4-coord. × 1 6-coord. × 2 (5.3)	4-coord. × 6 6-coord. × 2 (4.5)	4-coord. × 3 (4)
S	6-coord. × 1 (6)	4-coord. × 1 6-coord. × 2 (5.3)	6-coord. × 6 (6)	6-coord. × 2 (6)
P	6-coord. × 1 (6)	8-coord. × 2 (8)	8-coord. × 3 12-coord. × 1 (9)	12-coord. × 1 (12)
space group	*P*3*m*1	*Pm*	*P*6*mm*	*P*6*mm*

[a] The numbers in the parentheses represent the average coordination numbers (ACN) for the three components.

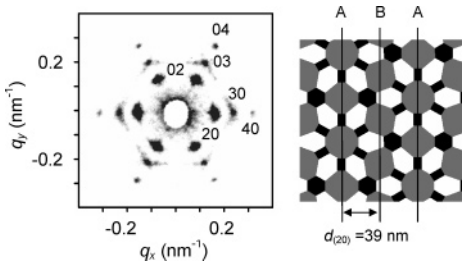

Figure 4. Microbeam SAXS pattern of $I_{1.0}S_{1.8}P_{2.0}$ (left) and the corresponding schematic tiling structure (right).

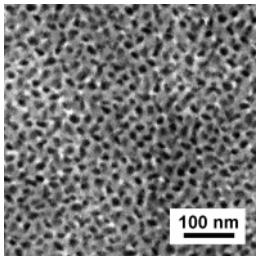

Figure 5. TEM image of the $I_{1.0}S_{1.8}P_{3.2}$ sample.

12-coordinated domains, respectively, is classified as the (4.6.12) Archimedean tiling pattern, as shown in Figure 3d.

On the other hand, two types of nanodomains with different sizes and shapes are formed by the same components in the tiling patterns of $I_{1.0}S_{1.8}P_{1.6}$ and $I_{1.0}S_{1.8}P_{2.0}$. Therefore, these tiling patterns cannot be assigned as any of the Archimedean tiling patterns, although they are apparently periodic. In the pattern of $I_{1.0}S_{1.8}P_{1.6}$, both I and S consist of the 4- and 6-coordinated domains and have equivalent coordination numbers. There is one 4-coordinated domain and two 6-coordinated domains for the component I and S in a unit cell (depicted by dotted lines in Figure 3b). Therefore, the average coordination numbers (ACN) of the components I and S are 5.3 (= (4 × 1 + 6 × 2)/3). For component P, two types of 8-coordinated domains under different environments are contained within the unit cell. Table 3 summarizes the tiling characteristics for the three components in a unit cell for the star polymers of the $I_{1.0}S_{1.8}P_X$ type. The numbers in the parentheses represent the ACN for these components, which are defined as the arithmetic means of the side numbers of the polygons as mentioned above. If the ACNs are used, the tiling pattern of $I_{1.0}S_{1.8}P_{1.6}$ is described as [5.3, 5.3, 8]. This tiling pattern has a 2-fold symmetry, which has never before been observed in the tiling patterns of ABC star-shaped terpolymers.

For the tiling pattern of $I_{1.0}S_{1.8}P_{2.0}$, components I and P each consist of two types of domains, while the same 6-coordinated domains can be recognized for component S, as shown in Figure 3c. Component P consists of 8- and 12-coordinated domains, and the dodecagonal P domain is surrounded by the six octagonal P domains, forming a hexagonal arrangement. Prior to this work, the complex tiling pattern described as [4.5, 6, 9] had not been reported experimentally or theoretically. In addition to the TEM observation, the [4.5, 6, 9] tiling pattern was also characterized by the microbeam SAXS measurement in the reciprocal lattice space. Figure 4 shows the microbeam SAXS pattern of $I_{1.0}S_{1.8}P_{2.0}$ and the corresponding *d*-spacing in real space. This SAXS pattern has 6-fold symmetry, which is consistent with the [4.5, 6, 9] tiling pattern having the hexagonal lattice. In the SAXS pattern, the first-order reflections are almost invisible. This could be due to the fact that the scattering power of the plane A (as designated in Figure 4) is comparable to that of the plane B because the 8- and 12-coordinated domains of the component P are almost the same size. Component P has the largest domain size and the highest electron density. These two characteristics exert a strong influence on the SAXS pattern. The 39 nm $d_{\{20\}}$-spacing determined by the SAXS pattern agrees well with the estimated value of approximately 40 nm, derived from the TEM image.

The ACNs of the four tiling patterns in Figure 3 are directly related to the volume ratio of component P. The ACN of component P increases (6 → 8→ 9 → 12) with an increase of the indicator *X*, which is accompanied by a decrease in the ACN of the component I (6 → 5.3 → 4.5 → 4), while that of the component S remains essentially constant (6 → 5.3 → 6 → 6).

When *X* equals 3.2, the periodic tiling pattern is suddenly transformed to a disorganized structure in which the three components remain distinct, as shown in Figure 5. According to this TEM image, the I domains are surrounded by the S domains in the matrix of the P domain with very poor periodicity. It appears that the structure is not cylindrical because the side views of the cylinder arrays do not appear in the TEM observation. It is obvious that the cylindrical structure is no longer retained due to the dominantly high volume fraction of the component P when *X* is larger than 3.2. A detailed discussion of this structure will be reported elsewhere.

Two-Dimensional Tiling Patterns of $I_{1.0}S_YP_{2.0}$. To investigate the universality of the systematic variation of the ACN, the tiling patterns of the blend sample series of the type $I_{1.0}S_YP_{2.0}$ were characterized and compared. In this blend sample series, macrophase separation was not observed by TEM because the molecular weights of the homopolymers added were quite low. TEM images of the $I_{1.0}S_YP_{2.0}$ star-based blend samples with *Y* of 1.3, 1.6, 2.3, and 2.7, and the corresponding schematic tiling patterns, are shown in Figure 6. The coordination characteristics for this series are listed in Table 4. The TEM image of the [4.5, 6, 9] tiling pattern is omitted from Figure 6 since it has already been shown in Figure 3c. The tiling patterns of $I_{1.0}S_{1.3}P_{2.0}$ (Figure 6a) and $I_{1.0}S_{2.7}P_{2.0}$ (Figure 6d) can be simply classified as the Archimedean tiling patterns (4.6.12) and (4.8.8), respectively.

In the tiling pattern for $I_{1.0}S_{1.6}P_{2.0}$, both component I and S consist of the 4- and 6-coordinated domains and the two are equivalent to each other in terms of coordination numbers, while component P has the same 10-coordinated domain arrangement. This [5, 5, 10] tiling pattern also exhibits 2-fold symmetry,

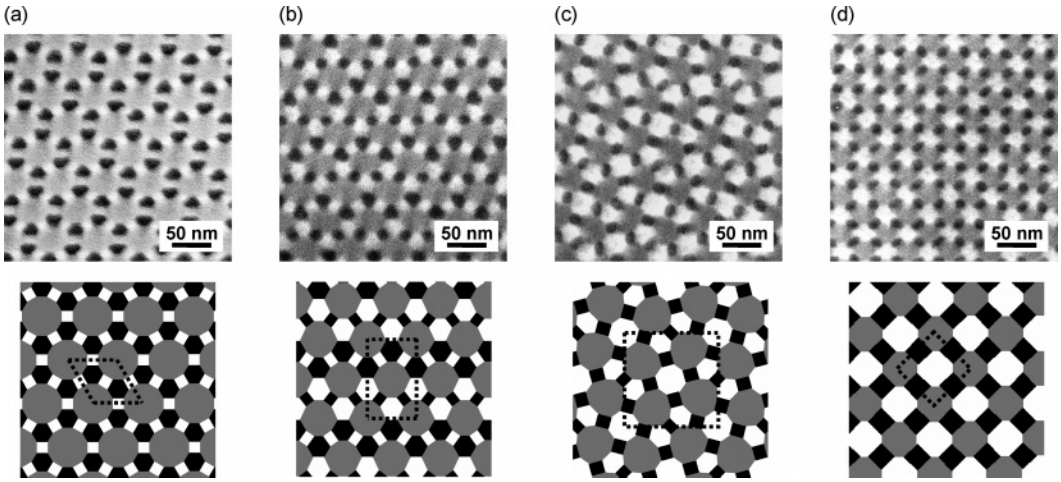

Figure 6. TEM images of the ISP star-based blend samples (top) and the corresponding schematic tiling patterns (bottom): (a) $I_{1.0}S_{1.3}P_{2.0}$, (b) $I_{1.0}S_{1.6}P_{2.0}$, (c) $I_{1.0}S_{2.3}P_{2.0}$, (d) $I_{1.0}S_{2.7}P_{2.0}$.

Table 4. Characteristics of the Tiling Patterns for the Star Polymers of the $I_{1.0}S_YP_{2.0}$ Series[a]

$I_1S_YP_{2.0}$	$Y = 1.1, 1.3$	$Y = 1.5, 1.6$	$Y = 1.8, 2.0$	$Y = 2.2, 2.3, 2.4$	$Y = 2.7$
I	6-coord. × 2 (6)	4-coord. × 2 6-coord. × 2 (5)	4-coord. × 6 6-coord. × 2 (4.5)	4-coord. × 10 (4)	4-coord. × 2 (4)
S	4-coord. × 3 (4)	4-coord. × 2 6-coord. × 2 (5)	6-coord. × 6 (6)	6-coord. × 4 8-coord. × 2 (6.7)	8-coord. × 1 (8)
P	12-coord. × 1 (12)	10-coord. × 2 (10)	8-coord. × 3 12-coord. × 1 (9)	10-coord. × 4 (10)	8-coord. × 1 (8)
space group	*P6mm*	*Pm*	*P6mm*	*P4gm*	*P4mm*

[a] The numbers in the parentheses represent the average coordination numbers (ACN) for the three components.

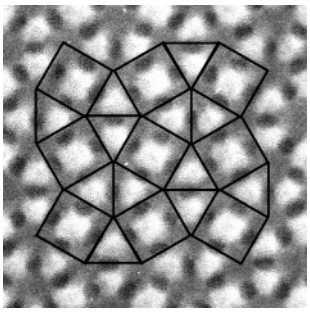

Figure 7. (3.3.4.3.4) tiling manner superimposed on the [4, 6.7, 10] tiling pattern.

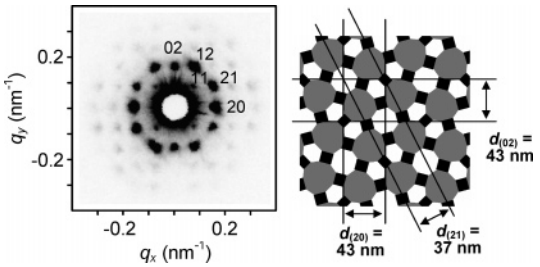

Figure 8. Microbeam SAXS pattern of $I_{1.0}S_{2.3}P_{2.0}$ (left) and the corresponding schematic tiling structure (right).

which is similar to the [5.3, 5.3, 8] tiling pattern for $I_{1.0}S_{1.8}P_{1.6}$ in Figure 3b.

In the tiling pattern for $I_{1.0}S_{2.3}P_{2.0}$, component I has two types of 4-coordinated domains and component S consists of 6- and 8-coordinated domains. Because there are four 6-coordinated domains and two 8-coordinated domains in a unit cell, the ACN of the S domains is 6.7, while component P has the same 10-coordinated domain arrangement. Thus, the tiling pattern for $I_{1.0}S_{2.3}P_{2.0}$ is described as [4, 6.7, 10] using the ACN. By applying the imaginary tiling scheme shown in Figure 7, this pattern has also been assigned as (3.3.4.3.4), which represents another example of an Archimedean tiling pattern.[13] In this tiling scheme, the equilateral triangles and the squares are centered on the 6- and 8-coordinated S domains, respectively. Figure 8 shows the microbeam SAXS pattern of the $I_{1.0}S_{2.3}P_{2.0}$ and the corresponding *d*-spacing drawn in a schematic model for the [4, 6.7, 10] pattern. In the SAXS pattern, the {20} and {21} reflections are clearly observed in addition to the {11} reflections,[15] indicating a 4-fold symmetry consistent with the (3.3.4.3.4) tiling pattern that has a square lattice. Although the {10} reflections cannot be confirmed from the scattering maxima near the beamstop, extinction is expected from the two-dimensional space group for the symmetry of the (3.3.4.3.4) tiling pattern, or *P4gm*. In addition, the $d_{\{20\}}$-spacing value of 43 nm, determined by the scattering experiment, is in good agreement with the TEM result of approximately 40 nm.

The ACNs for $I_{1.0}S_YP_{2.0}$ are also related to the volume ratio of component S. As shown in Table 4, the ACN for component S increases monotonically (4 → 5 → 6 → 6.7 → 8) with an increase of the *Y* value and a decrease in the value of component I (6 → 5 → 4.5 → 4 → 4), while the value of the component P varies unsystematically (12 → 10 → 9 → 10 → 8).

Discussion

It is well-established that nanophase-separated structures of linear block copolymers can be dominantly determined by molecular parameters such as chain lengths or volume fractions of component polymers and the polymer−polymer interactions. In the structural formation process, the counterbalanced effects resulting from interfacial and chain deformation energies play essential roles to govern morphology. As in the case of linear block systems, the tiling patterns formed by ABC star polymers can be effectively determined by molecular parameters and

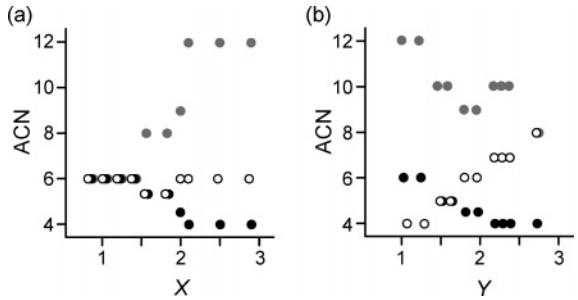

Figure 9. ACN variations for the I (black), S (white), and P (gray) components as a function of *X* or *Y*: (a) $I_{1.0}S_{1.8}P_X$, (b) $I_{1.0}S_YP_{2.0}$.

polymer−polymer interactions. In the latter system, however, the interfacial curvatures are not directly affected by the volume fractions and the polymer−polymer interactions because no junction points exist at the polymer−polymer interface. As a result, the requirements of minimizing interfacial area and optimizing chain stretching at fixed volume fractions determines the resultant tiling patterns.

A simple phase transition rule can be extrapolated from the variation of the ACNs for the $I_{1.0}S_{1.8}P_X$ and $I_{1.0}S_YP_{2.0}$ series. Figure 9 shows the plots of the ACNs for the component I (black), S (white), and P (gray) as a function of *X* or *Y* for $I_{1.0}S_{1.8}P_X$ (a) and $I_{1.0}S_YP_{2.0}$ (b), respectively. Figure 9 indicates that the ACNs of the variable components (P for $I_{1.0}S_{1.8}P_X$ and S for $I_{1.0}S_YP_{2.0}$) increase monotonically with increasing values of *X* or *Y*, while the ACNs of the component I, whose volume fractions are smaller than those of the remaining components in both cases, exhibits a stepwise decrease with increasing values of *X* or *Y*. This phase transition rule is supported by the requirement to minimize the chain deformation energies, or the components having large volume fractions occupy large domains with high coordination numbers, while the component having small volume fractions occupy small domains with low coordination numbers.

A similar but distinct phenomenon was observed in previous work for $I_{1.0}S_{1.0}P_X$, where component P was the ascendant component and both component S and component I were descendant components. In short, the ACN for component P monotonically increased (6 → 8 → 10 → 12) with an increase of the indicator *X*, and the ACN for component S decreased (6 → 4 → 4 → 4), while the ACN of component I was varied (6 → 8 → 6.7 → 6). In this case, the ACN of the component S first dropped from 6 to the minimum possible ACN of 4, while the ACN of component I increased from 6 to 8 although the volume fractions of the components I and S were the same. After the ACN of component S had reached 4, the ACN for component I decreased monotonically (8 → 6.7 → 6). This phenomenon can be explained by taking into account not only the volume fractions but also the relative magnitude of polymer−polymer interactions. The interactions between components S and P is smaller than the interactions between components I and P, or $\chi_{SP} < \chi_{IP}$.[40] Component P preferentially contacts component S rather than component I, and consequently, component S is divided into smaller domains with low coordination numbers in order to gain P/S interfacial area instead of P/I interfacial area. With further increases of *X*, however, the descendant component must be switched to I because the ACN of S attains the minimum value of 4.

As mentioned above, the tiling patterns observed in the series of the ISP-star polymers have been found to change systematically according to a simple rule involving the ACN defined in this work. When the volume ratio of a given component is increased, its ACN monotonically increases and the component becomes the ascendant component. On the other hand, the minor component, which is determined not only by volume fractions but also by interactions with the ascendant component, becomes the descendant component and its ACN undergoes a monotonic decreases. The ACN of the third component does not vary simply. However, if the ACN of the minor component has reached 4, which is the minimum ACN of any phase, the ACN of the third component begins to decrease monotonically. Thus, ACNs are very useful indicators for describing and predicting systematic transitions of tiling patterns formed by ABC star-shaped terpolymers.

By overlooking the phase transition for the two series, it can be seen that four new tiling patterns [5.3, 5.3, 8], [4.5, 6, 9], [5, 5, 10], and [4, 6.7, 10] have been identified in the present study. The structural features of tiling patterns [4.5, 6, 9] and [4, 6.7,-10] will be discussed in more detail. The common feature of these complex tiling patterns arises from the fact that the polymer coils of at least one component are partitioned into the two different domains. These structures may have inevitably appeared in the domain formation process as the polymer chains undergo periodic self-assembling to minimize the total free energy. On the contrary, provided that each component must form the same domains, only three Archimedean tiling patterns can exist: (6.6.6), (4.8.8), and (4.6.12).[17] In the $I_{1.0}S_{1.8}P_X$ system, the direct transition from [6, 6, 6] to [4, 6, 12] would not be possible due to the significant difference between volume fractions suitable for [6, 6, 6] and [4, 6, 12]. Therefore, the [5.3, 5.3, 8] and [4.5, 6, 9] patterns emerge as the most stable phases between the [6, 6, 6] and [4, 6, 12] tiling patterns. Thus, the existence of these complex tiling patterns is acceptable for two-dimensional tiling transitions.

In the [4.5, 6, 9] tiling pattern, the octagonal and dodecagonal domains for component P are indicated to be almost the same size by the TEM and SAXS results. This interesting observation is attributed to the requirement for minimization of the surface area of the dominant P component against the I and S components. Therefore, singular domains having similar shapes and sizes might be created for component P in this pattern. Similarly, the sizes and shapes of the P domains are uniformly determined in the other tiling patterns observed in this study where the P components are dominant.

Another complex but periodic tiling pattern, (3.3.4.3.4), has been successfully observed in the present study. This pattern is associated with the [4, 6.7, 10] arrangement using the ACN concept, which is actually one counterpart of a structure reported in the previous work, which is described as [6.7, 4, 10] wherein component I and S are interchanged. Recently, such (3.3.4.3.4) tiling patterns have also been found by Monte Carlo simulations[23] in addition to [5.3, 5.3, 8] and [5, 5, 10] tiling patterns.[17] These findings provide reliable evidence of existence of these complex tiling patterns.

In summary, the systematic transitions of the two-dimensional tiling patterns have been studied extensively for two series of star-shaped terpolymers: $I_{1.0}S_{1.8}P_X$ and $I_{1.0}S_YP_{2.0}$. Investigation of the influence of variations of the composition of *X* or *Y* on the periodic bulk structures has enabled us to conclude that the transition can be effectively described by the concept of the average coordination number, which is defined as the mean value of the side numbers of polygonal domains formed by each component. When *X* is increased, the ACN of P for $I_{1.0}S_{1.8}P_X$ increases monotonically, accompanied by a decrease in ACN of component I. Similarly, the ACN of S for $I_{1.0}S_YP_{2.0}$ increases if *Y* is increased, while the ACN of I decreases.

In determining this transition rule, four new tiling patterns have been observed for the $I_{1.0}S_{1.8}P_X$ and $I_{1.0}S_YP_{2.0}$ samples: [5.3, 5.3, 8], [4.5, 6, 9], [5, 5, 10], and [4, 6.7, 10]. The [4, 6.7, 10] pattern corresponds to the (3.3.4.3.4) Archimedean tiling pattern, and the general ability of star-shaped terpolymers to form this highly complex structure has been proven herein.

Furthermore, we can predict new tiling patterns both theoretically and experimentally by applying the ACN concept to ABC star-shaped terpolymers. Recently, Dotera et al. have performed a Monte Carlo simulation and observed a two-dimensional dodecagonal quasicrystal formed by an ABC star-shaped terpolymer.[22]

Acknowledgment. This work was partially supported by a research grant from the 21st Century COE Program under support from the Japan Society for the Promotion of Science (JSPS) entitled "Nature-Guided Materials Processing" at the School of Engineering, Nagoya University. K.H. and Y.M. gratefully acknowledge support under this grant. This work was also partly supported by a grant from PRESTO, Japan Science and Technology Corporation (JST), for which A.T. gratefully acknowledges support. The SAXS experiments were performed under the approval of SPring-8 (proposal no. 2006A1238).

References and Notes

(1) Molau, G. E. In *Block Copolymers*; Agarwal, S. L., Ed.; Plenum Publishing: New York, 1970.
(2) Norshay, A.; McGrath, J. E. Block Copolymers. In *Overview and Critical Survey*; Academic Press: New York, 1977.
(3) Riess, G. *Encyclopedia of Polymer Science and Engineering*; John Wiley & Sons: New York, 1986.
(4) Galllot, B. R. M. *Adv. Polym. Sci.* **1978**, *29*, 85.
(5) Hadjichristidis, N.; Iatrou, H.; Behal, S. K.; Chludzinski, J. J.; Disko, M. M.; Garner, R. T.; Liang, K. S.; Lohse, D. J.; Milner, S. T. *Macromolecules* **1993**, *26*, 5812.
(6) Okamoto, S.; Hasegawa, H.; Hashimoto, T.; Fujimoto, T.; Zhang, H.; Kazama, T.; Takano, A.; Isono, Y. *Polymer* **1997**, *38*, 5275.
(7) Sioula, S.; Hadjichristidis, N.; Thomas, E. L. *Macromolecules* **1998**, *31*, 5272.
(8) Sioula, S.; Hadjichristidis, N.; Thomas, E. L. *Macromolecules* **1998**, *31*, 8429.
(9) Huckstadt, H.; Gopfert, A.; Abetz, V. *Macromol. Chem. Phys.* **2000**, *201*, 296.
(10) Yamauchi, K.; Takahashi, K.; Hasegawa, H.; Iatrou, H.; Hadjichristidis, N.; Kaneko, T.; Nishikawa, Y.; Jinnai, H.; Matsui, T.; Nishioka, H.; Shimizu, M.; Furukawa, H. *Macromolecules* **2003**, *36*, 6962.
(11) Takano, A.; Wada, S.; Sato, S.; Araki, T.; Hirahara, K.; Kazama, T.; Kawahara, S.; Isono, Y.; Ohno, A.; Tanaka, N.; Matsushita, Y. *Macromolecules* **2004**, *37*, 9941.
(12) Abetz, V.; Jiang, S. *e-Polymers* **2004**, no. 054.
(13) Takano, A.; Kawashima, W.; Noro, A.; Isono, Y.; Tanaka, N.; Dotera, T.; Matsushita, Y. *J. Polym. Sci., Part B: Polym. Phys.* **2005**, *43*, 2427.
(14) Yamauchi, K.; Akasaka, S; Hasegawa, H.; Iatrou, H.; Hadjichristidis, N. *Macromolecules* **2005**, *38*, 8022.
(15) Hayashida, K.; Kawashima, W.; Takano, A.; Shinohara, Y.; Amemiya, Y.; Nozue, Y.; Matsushita, Y. *Macromolecules* **2006**, *39*, 4869.
(16) Bohbot-Raviv, Y.; Wang, Z.-G. *Phys. Rev. Lett.* **2000**, *85*, 3428.
(17) Gemma, T.; Hatano, A.; Dotera, T. *Macromolecules* **2002**, *35*, 3225.
(18) He, X.; Huang, L.; Liang, H.; Pan, C. *J. Chem. Phys.* **2002**, *116*, 10508.
(19) He, X.; Huang, L.; Liang, H.; Pan, C. *J. Chem. Phys.* **2003**, *118*, 9861.
(20) Tang, P.; Qiu, F.; Zhang, H.; Yang, Y. *J. Phys. Chem. B* **2004**, *108*, 8434.
(21) Lu, T.; He, X.; Liang, H. *J. Chem. Phys.* **2004**, *121*, 9702.
(22) Birshtein, T. M.; Polotsky, A. A.; Abetz, V. *Macromol. Theory Simul.* **2004**, *13*, 512.
(23) Dotera, T.; Gemma, T. *Philos. Mag.* **2006**, *86*, 1085.
(24) Grunbaum, B.; Shephard, G. C. In *Tilings and Patterns;* Freeman: New York, 1986.
(25) Hashimoto, T.; Tanaka, H.; Hasegawa, H. *Macromolecules* **1990**, *23*, 4378.
(26) Tanaka, H.; Hasegawa, H.; Hashimoto, T. *Macromolecules* **1991**, *24*, 240.
(27) Winey, K. I.; Thomas, E. L.; Fetters, L. J. *Macromolecules* **1991**, *24*, 6182.
(28) Shull, K. R.; Winey, K. I. *Macromolecules* **1992**, *25*, 2637.
(29) Koizumi, S.; Hasegawa, H.; Hashimoto, T. *Macromolecules* **1994**, *27*, 6532.
(30) Winey, K. I.; Thomas, E. L.; Fetters, L. J. *Macromolecules* **1992**, *25*, 2645.
(31) Epps, T. H., III; Chatterjee, J.; Bates, F. S. *Macromolecules* **2005**, *38*, 8775.
(32) Matsen, M. W. *Macromolecules* **1995**, *28*, 5765.
(33) Matsen, M. W. *Phys. Rev. Lett.* **1995**, *74*, 4225.
(34) Milner, S. T.; Xi, H. *Macromolecules* **1996**, *29*, 2404.
(35) Dotera, T. *Phys. Rev. Lett.* **2002**, *89*, 4225.
(36) Takano, A.; Kadoi, O.; Hirahara, K.; Kawahara, S.; Isono, Y.; Suzuki, J.; Matsushita, Y. *Macromolecules* **2003**, *36*, 3045.
(37) Matsushita, Y.; Watanabe, J.; Katano, F.; Yoshida, Y.; Noda, Y. *Polym. J.* **1996**, *37*, 321.
(38) Zieglar, K.; Dislich, H. *Chem. Ber.* **1957**, *90*, 1107.
(39) Takano, A.; Kondo, K.; Ueno, M.; Ito, K.; Kawahara, S.; Isono, Y.; Suzuki, J.; Matsushita, Y. *Polym. J.* **2001**, *33*, 732.
(40) Unpublished data. According to recent neutron scattering experiments based on poly(isoprene-d8-*block*-2-vinylpyridine) with M of 4 k (by SEC) at high temperatures up to 220 °C, we were not able to reach the disordered state under the conditions employed. This result means that χIP is much higher than χIS and χSP.

MA0618474